THE JOURNAL OF PHYSICAL CHEMISTRY C

ARTICLE

pubs.acs.org/JPCC

Exohedral Hydrogen Chemisorption on a Carbon Nanotube: The Clustering Effect

Wanda Andreoni,*[,†,‡,§] Alessandro Curioni,[§] Jaap M. H. Kroes,[†] Fabio Pietrucci,[‡] and Oliver Gröning[∥]

[†]Institut de Théorie des Phénomènes Physiques, and [‡]Centre Européen de Calcul Atomique et Moléculaire (CECAM), Ecole Polytechnique Fédérale de Lausanne, Switzerland

[§]IBM Research − Zurich, Rüschlikon, Switzerland

[∥]Swiss Federal Laboratories for Materials Testing and Research (EMPA), Dübendorf, Switzerland

Supporting Information

ABSTRACT: Density functional theory-based calculations of the (10,0) zigzag single-walled carbon nanotube with hydrogen chemisorbed exohedrally show that electron pairing and strain minimization lead hydrogen atoms to cluster and preferentially sit in axial configurations. This tendency to confine in highly ordered configurations contrasts with the results we obtain when we employ the widely used force field AIREBO that predicts a preference for a sparse hydrogen distribution. The nature of the frontier orbitals is significantly dependent on the specific configuration of the adsorbate, being either unperturbed delocalized states of the bare nanotube or localized "impurity" states. The infrared absorption spectrum calculated for a model with hydrogen bound both on the surface and at the edges of the nanotube allows an unambiguous assignment of the characteristic features observed for hydrogenated single-walled carbon nanotubes.

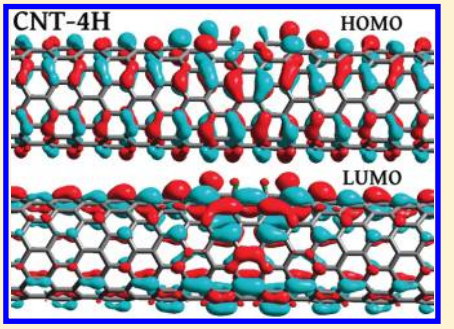

Since their discovery,[1] carbon nanotubes (CNTs) have continued to attract a huge interest worldwide because of their peculiar physical and chemical properties.[2] In particular, the adsorption behavior of a single-wall carbon nanotube (SWNT), be it chemi- or physisorption, substantially differs from that of graphite or fullerenes, and critically depends on whether the inner or outer surface is exposed and on the tube chirality and diameter. Understanding its characteristics and being able to predict relevant adsorption configurations are important for complementing ongoing experimental efforts in developing covalent sidewall functionalization[3] and applications of CNTs as gas sensors[4] and hydrogen storage materials.[5] Although more attention has been devoted to the interaction of CNTs with molecular hydrogen, detailed and systematic experimental studies of the effects of hydrogenation by atomic hydrogen or hydrogen plasma are also available.[6−10] For example, it was shown that stable hydrogenation by atomic hydrogen can be obtained to a degree depending on the nanotube diameter (100% for a 2 nm diameter).[9]

This state of affairs contrasts with the limited number of investigations carried out with theoretical approaches. These studies have focused either on the detailed, also quantitative, characterization of exo- and endochemisorption of one[11−13] or two[13−15] hydrogen atoms only or on the prediction of the effects of hydrogen adsorption at high concentration[16−20] and the investigation of possible storage mechanisms.[17,18,20]

In particular, ab initio and PM3 calculations[11] performed on a series of armchair (n,n) SWNTs with one chemisorbed hydrogen showed that the tube reactivity is higher at the convex surface than at the concave one and decreases with increasing diameter. Moreover, density functional theory (DFT)-based calculations[12] of one H chemisorption on (5,5) and (10,0) SWNTs emphasized that this involves strong local structural changes and relatively large binding energies (1−1.5 eV), and that the use of the hybrid exchange-correlation (xc) functional HSE03[21] does not modify the binding energy values obtained with the nonhybrid PBE functional,[22] but that it is necessary to represent the variation of the band gaps induced by chemisorption correctly. Other DFT studies,[13−16] carried out on zigzag SWNT models, focused on the adsorption of two hydrogens resulting from the dissociation of a molecule. In particular, they revealed that one chemisorbed hydrogen induces the formation of a wave-like modulation of the charge density at the Fermi level, with alternate cusps and nodes at the carbon positions, and that the cusps correspond to energy minima for the two-hydrogen adsorbate. The lowest energy configuration has both adsorbed atoms on the sites of a double bond. With the exclusion of the latter, the other (metastable) configurations are shown to give rise to double peaks in the local density of states, which is proposed to explain the abundance of double-peak structures in the measured scanning tunneling spectrum (dI/dV vs bias voltage).[14]

In this Article, we first examine to what extent the chemisorption of several hydrogen atoms on a CNT is "correlated" and what the underlying mechanism is. We use DFT calculations in the PBE approximation[22] of the xc functional and show that successive hydrogen chemisorption follows a pattern, which can be unambiguously explained on the basis of quantum-mechanical

Received: September 3, 2011
Revised: November 10, 2011
Published: November 11, 2011

Table 1. Geometry Characteristics and Binding Energies (E_B, in eV) per H Atom for the Low-Energy Configurations in Figure 1: Bond Lengths d(CH), d(CC), d(CC*) (in Å), and Bond Angles (α,β) and Pyramidalization (θ) Angles (in deg)[a]

n (conf)	E_B	d (C−H)	d (C−C$_x$*)	d (C−C*)	α (C*CH)	β (C*CC*)	θ
1	1.64[b]	1.120	1.501	1.522	108; 106	109; 114	17.0
ref.11-PBE	1.5[c]	1.116	1.502	1.534	108.5; 107.5	106.4; 113.3	
ref.11-HSE03	1.5[c]	1.085	1.493	1.522	108.5; 107.6	106.3; 113.2	
2(a)	2.13	1.109	1.558	1.526	106	106; 116	16.0
3(a)	2.13	1.113	1.556 *1.500*	1.525	106.5	106; 115	16.5
4(a)	2.28	1.109	1.560	1.526	107	104; 116	16.6
5(a)	2.235	1.112	1.560; *1.493*	1.526	107	105; 116	16.7
5(b)	2.22	1.110	1.559; *1.498*	1.516; *1.583*	104; 106	113; 114	14.6
6(a)	2.34	1.109	1.556	1.527	107	104; 116	16.7
7(a)	2.27	1.111	1.557; *1.498*	1.527	107	104; 116	16.8
8(a)	2.385	1.109	1.555	1.527	107	103; 116	16.8

[a] For $n > 1$, average values are given. C atoms are bound to H atoms, C* atoms only to C atoms; among them, C$_x$*'s are the atoms closest to the C's in the bare nanotube (d = 1.416 Å). C$_x$*'s are all chemisorption sites (C) for even "n"; if not (odd "n"), distances are in italics. [b] This E_B value includes spin polarization that contributes 0.10 eV. [c] These values were obtained by fully relaxing a model containing 40 carbon atoms in the periodically repeated (fixed) unit cell and using a mesh of at least 80 k-points in the first Brillouin Zone; the basis set was 6-31G for C and 6-31G** for H.

Table 2. Chemisorption Configurations for n = 1−4: PBE Results (in eV) for Binding Energies (E_B) per H Atom and Corresponding Loss Due to Deformation (E_D) and "Confinement" Gain (E_C)[a]

	n (conf)									
	1	2(a)	2(b)	3(a)	3(b)	3(c)	4(a)	4(b)	4(c)	4(d)
E_B (QM)	1.64 [1.56] *1.65*	2.13 [1.97] *2.16*	1.85 [1.90] *1.87*	2.13 [1.99] *2.14*	2.05 [1.97] *2.09*	1.73	2.28 [2.11] *2.29*	2.23 [2.07] *2.26*	1.88	1.85
E_D (QM)	−0.76	−0.52	−0.76	−0.84	−0.82	−0.83	−0.86	−0.73	−0.86	−0.73
E_C (QM)		0.48$_S$ [0.41] *0.51*	0.21 [0.34] *0. 23*	0.48$_S$ [0.43] *0.49*	0.41 [0.41] *0.44*	0.09	0.64 [0.55] *0.64*	0.59 [0.51] *0.62*	0.24	0.21
E_B (A)	3.13	2.82	3.12	2.92	2.82	2.91	2.82	2.79	2.40	3.13
E_D (A)	−1.23	−1.08	−1.25	−1.13	−1.06	−1.22	−1.06	−1.05	−1.12	−1.26
E_C (A)		−0.31	−0.01	−0.21	−0.31	−0.22	−0.31	−0.33	−0.73	0.00

[a] QM = DFT-PBE; A = AIREBO. Configuration labels correspond to those of Figure 1. Values in italic are obtained with the BLYP xc functional, and in square brackets from calculations using PBC (see text). All of these values are per H atom.

arguments. The most important finding is the preference for clustering rather than sparse configurations, which we confirm with additional calculations performed within other xc functionals: the BLYP[23] and the hybrid PBE0.[24] We further explore whether this tendency can be detected from the observation of either electronic or vibrational spectra. The nature of the Kohn−Sham states near the band edges is thus analyzed also with the aim of verifying the validity of previous interpretations of experimental data.[14] The vibrational spectrum is also evaluated for one of these systems (CNT-4H), which allows us to assess the nature of the vibrational modes giving rise to characteristic peaks in the infrared spectra of hydrogenated single-walled CNTs.[6,8]

We then use our ab initio results as an example for the verification of whether classical potentials reproduce the chemistry of the CNT-hydrogen system. This test is important because currently the study of large-size systems of interest for technological applications cannot be performed with DFT-based methods and requires the use of reliable classical potentials. In particular, we investigate the Adaptive Intermolecular Reactive Empirical Bond Order (AIREBO) potential[25] and apply it to determine optimal adsorption configurations.

METHODS

We present a series of calculations on the zigzag (10,0) carbon SWNT. As it will be specified case by case, in most calculations the tube was represented by an isolated model consisting of 240 carbon atoms; those at the ends are saturated by hydrogen atoms (two each).[26] Additional calculations were made for models with 360 carbon atoms in a periodically repeated orthorhombic unit cell of edges a = 38.40 Å and $b = c$ = 21 Å.

The study discussed here for the structural, electronic, vibrational properties, and binding energies relies on the Kohn−Sham approach to DFT. In particular, the computational scheme includes norm-conserving l-dependent Martins−Troullier pseudopotentials,[27] and a plane-wave expansion of the wave functions up to a 55 Ry cutoff. Systematic calculations are presented using both PBE[22] and BLYP[23] approximations for the exchange-correlation functionals (including spin-polarization for open-shell configurations). For the 1- and 2-hydrogens chemisorption, additional calculations are reported using the hybrid PBE0[24] exchange-correlation functionals and the PBE pseudopotentials. Only the lowest spin multiplicity electron states were considered. Wave function optimization was performed with the preconditioned conjugate-gradients method, geometry optimization with the L-BFGS method,[28] and vibrational spectra were obtained in the linear-response theory scheme.[29] All of these QM calculations used the CPMD code.[30] In the calculations on the H-passivated model, the artificial periodic images were decoupled using the Hockney's Poisson solver.[31] In the calculation of

dx.doi.org/10.1021/jp208501b |J. Phys. Chem. C 2012, 116, 269–275

Table 3. Chemisorption Configurations for $n = 5-8$: Results (in eV) for Binding Energies (E_B) per H Atom and Corresponding Loss Due to Deformation (E_D) and "Confinement" Gain (E_C)[a]

	n (conf)											
	5(a)	5(b)	5(c)	6(a)	6(b)	6(c)	7(a)	7(b)	8(a)	8(b)	8(c)	8(d)
E_B(QM)	2.22 *2.22*	2.23$_5$*2.24*	2.22	2.34 *2.35*	2.31 *2.33*	2.26	2.27 *2.28*	2.29 *2.31*	2.38$_5$*2.39*	2.35 *2.37*	2.33	1.92
E_D (QM)	−0.93	−0.65	−0.68	−1.18	−0.57	−0.59	−1.08	−0.97	−0.63	−0.89	−0.89	−1.68
E_C (QM)	0.58 *0.57*	0.59 *0.59*	0.58	0.70 *0.71*	0.67 *0.68*	0.62	0.63 *0.63*	0.65 0.66	0.74 *0.74*	0.71 *0.72*	0.69	0.28
E_B (A)	2.88	2.78	2.82	2.82	2.77	2.81	2.86	2.77	2.82	2.76	2.80	2.60
E_D (A)	−1.09	−1.03	−1.04	−1.05	−1.01	−1.03	−1.08	−1.01	−1.04	−0.99	−1.04	−1.41
E_C (A)	−0.25	−0.35	−0.31	−0.31	−0.36	−0.32	−0.27	−0.35	−0.31	−0.37	−0.33	−0.53

[a] QM = DFT-PBE; A = AIREBO. Values in italic are from BLYP calculations. All of these values are per H atom. Configuration labels correspond to those of Figure 1.

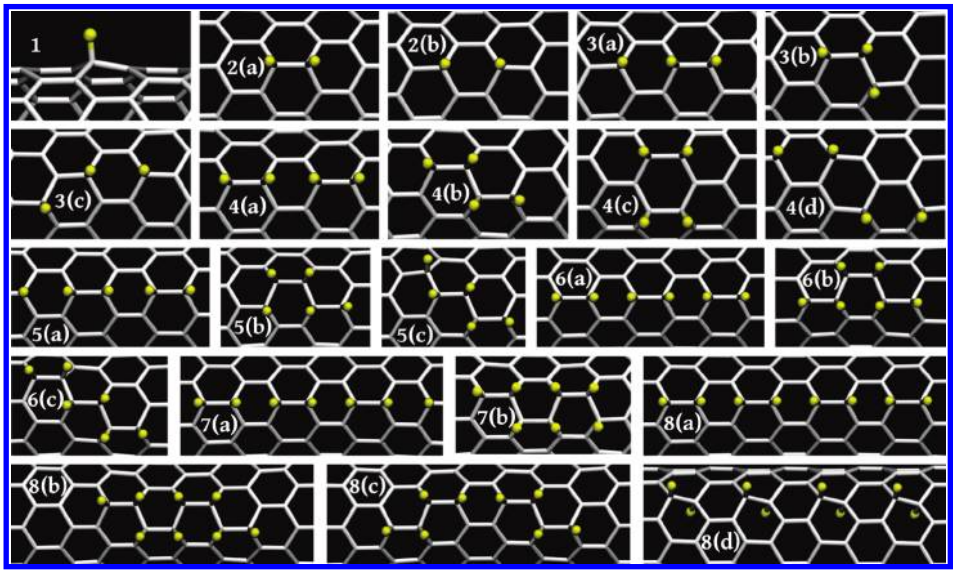

Figure 1. CNT-nH: All configurations considered here for the systems with $n = 1$ (side view) and $n = 2-8$ (top view). Note that in 8(d), both exohedrally and endohedrally chemisorbed hydrogens are present.

the periodically repeated system (referred to as PBC calculations), only the Γ point of the Brillouin Zone was taken into account.

In some cases (CNT-1H and CNT-2H), all-electron DFT calculations are also presented for the same model described above, representing an isolated nanotube, using the meta-hybrid M06 functional,[32] with the aug-cc-pvdz basis set. These computations employed the NWCHEM code.[33]

Classical potential-based calculations used the AIREBO force field[25] as implemented in the Lammps code.[34] Geometry optimization was obtained with the conjugate-gradients method and the Hessian matrix, using the finite differences procedure.

RESULTS AND DISCUSSION

We consider an isolated zigzag (10,0) SWNT and represent it with the H-passivated model described in the Methods. In Tables 1−3, we present results for the geometric characteristics and energies associated with the binding and the structural deformation induced by hydrogen chemisorption. In these tables, E_B is the binding energy per H atom defined as the opposite of the formation energy relative to the separate fragments (i.e., the CNT in its optimized geometry and isolated hydrogen atoms) at zero temperature ($E_B(n) = (E(\mathrm{CNT}) - E(\mathrm{CNT}+n\mathrm{H}))/n + E(\mathrm{H})$); E_D is the loss due to the deformation of the nanotube structure induced by chemisorption, that is, the energy difference between the bare CNT in its optimized geometry and in the one adopted in the CNT-nH system; and E_C is the "confinement" energy per H, the binding energy referred to the one of a configuration having far-away (noninteracting) H atoms ($E_C(n) = E_B(n) - E_B(1)$).

Figure 1 illustrates the system configurations that we calculated. For the CNT-1H and CNT-2H cases, Figure 2 shows the change of the Mulliken population (ΔMP) induced by chemisorption, which corresponds to the change of the local density of the occupied states at the carbon sites. This helps understand the binding mechanism.

The characteristics of the exohedral chemisorption of a single hydrogen atom on a SWNT are well-known: strong binding accompanied by rehybridization of the carbon states from sp^2-like to sp^3-like. This variation is reflected in the increase of the pyramidalization angle[35] at the adsorption site from 5° to 17° (Table 1). The top panel of Figure 2 displays the difference in Mulliken population (ΔMP) between the CNT-1H system and the bare nanotube. ΔMP is negative (−0.175) on the carbon (C_0) bound to hydrogen, as a consequence of the charge localization induced by the formation of the σ C−H bond. The strong

dx.doi.org/10.1021/jp208501b |J. Phys. Chem. C 2012, 116, 269–275

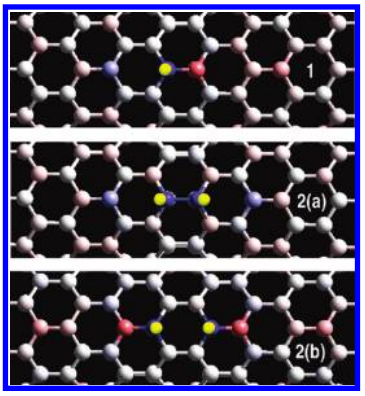

Figure 2. CNT-*n*H: Differential Mulliken population ΔMP for $n = 1$ (upper panel) and $n = 2$ (2(a) in the middle panel and 2(b) in the lower panel). Blue: ΔMP < 0. Red: ΔMP > 0. The color intensity decreases with decreasing value of |ΔMP|.

perturbation of the π-system induced by chemisorption creates a charge wave with a sizable partial charge localization on the carbon atom in the para position to C_0 along the axial direction (ΔMP = −0.02) and on the one in the ortho position (sharing a double bond in the absence of hydrogen) (ΔMP = 0.03). There the spin density accumulates; therefore, this site is kinetically favored for the attack of a second hydrogen. The resulting configuration for CNT-2H is the one labeled 2(a) in Figure 1. The deformation induced in the CNT structure (measured by E_D in Table 2) is weaker in 2(a) than in the configuration with the second hydrogen sitting on one of the other adjacent carbons (2(b)). As a consequence, the nucleophile addition in 2(a) is also thermodynamically favored. The difference in binding energy between 2(a) and 2(b) turns out to be 0.3 eV in both PBE and BLYP (Table 2). Further calculations using the hybrid PBE0[24] and the meta-hybrid M06[32] functional confirm this value. Our result is also in agreement with previous GGA calculations,[13−15] but the reason for it and the sizable difference from 2(b) were not explained earlier.

In the CNT-2H system, pair configurations are clearly strongly favored with respect to isolated chemisorption sites. We also verified that the E_C values change by less than 0.03 eV on passing from PBE to BLYP and even increase (but by less than 0.1 eV) from PBE to PBE0. We have considered a few possible configurations for subsequent hydrogen chemisorption, starting from the "dimer" in 2(a). As can be seen in Figure 1, the n(a) (n from 2 to 8) sequence corresponds to a linear chain parallel to the tube axis; the 2(a)-3(b)-4(b)-5(b)-6(b) to an armchair arrangement, and the 2(a)-3(b)-4(b)-5(c)-6(c) to a zigzag one. Characteristic changes in the environment of the chemisorption carbon sites are reported in Table 1 for the axial ordering, which is energetically favored for $n = 2−4$ (Table 2). The energy difference between the (a) and (b) isomers decreases for $n > 4$ (Table 3) and falls within the error introduced by the CNT termination of our model (∼0.01 eV). We have repeated some of the calculations on a (10,0) SWNT model of 360 carbon atoms using (fixed) PBC (see Methods). The trends and energy ranking remain unaltered. However, also these calculations cannot guarantee a higher accuracy and suffer from systematic errors. For example, hydrogen chemisorption on the carbon atoms of a "double bond" causes a lengthening of the tube in the H-passivated model, which is inhibited by the PBC constraint. By not allowing sufficient geometry relaxation to axial hydrogen sequences, these calculations tend to predict a slightly weaker bonding for the (a) structures and smaller (a)−(b) energy differences. These results are also reported in Table 2.

On the basis of the ΔMP distribution (Figure 2), one could speculate on the kinetically favored configurations. With the "dimer" in 2(a), one would predict that the next hydrogen sticks on one of the adjacent positions as in 3(b); likewise, starting with the dimer in 2(b), the next hydrogen is more likely to stick on one of the axial nearest neighbors as in 3(a). However, the (positive) values of ΔMP at the close empty sites are much smaller (0.003) in 2(a) than in 2(b) (0.027), and there is a negligible difference in the energy loss E_D due to structural deformation in the 3(a) and 3(b) isomers. As a consequence, the 3(a) configuration is thermodynamically favored. Electronic effects also dominate the ranking of the tetramer adsorbate: The comparison of 4(c) and 4(d) with 4(a) and 4(b), in which the H atoms are closer, demonstrates the crucial role of electron pairing. For $n = 5, 6, 7$, and 8, the (a) and (b) isomers are almost "energetically degenerate". The 8(d) isomer has mixed (symmetrically distributed) exo- and endohedral adsorption positions; it is remarkably less stable than the (a)−(c) structures because, as explained in ref 11, the binding is weaker on the concave than on the convex surface of the tube.[11−13]

The existence of a correlation between the hydrogen chemisorption sites was predicted in ref 14 as an electronic effect due to the formation of a charge wave at the Fermi level. Electron-pairing was considered[15] the predominant factor in determining the energetics of the CNT-2H isomers, and, on this basis, adsorbates consisting of dimers were predicted to dominate the configurations of hydrogenated CNTs.[15] Our calculations confirm that for an even number of hydrogen atoms, electron pairing is critical in driving them to closer distances, but that it is not necessarily the decisive factor in the ranking of close-by geometries. In the case of the CNT-2H (a) and (b) isomers, for example, that role is played by strain relaxation. An odd−even alternation can be recognized in the binding energies of the lowest-energy configurations, but only within 0.1 eV.

As can be seen in Tables 2 and 3, the AIREBO scheme does not reproduce the trends found in the DFT results and significantly overestimates both the binding strengths (on average at least 0.5 eV higher) and the energy losses E_D associated with the structural deformation of the tube induced by H addition. The effects of electron pairing are missed as well as the peculiarity of the "dimer" configuration on the CNT; as a consequence, most of the physicochemical characteristics of the CNT-*n*H systems cannot be correctly represented. In all cases, quantum-mechanical (QM) calculations predict a strong tendency of the hydrogen atoms to cluster ($E_C > 0$), whereas the AIREBO potential strongly favors the opposite behavior ($E_C < 0$), configurations with far-away chemisorption sites.

To understand to what extent the electronic structure reflects the structural characteristics of different configurations, we considered the Kohn−Sham (KS) spectrum of occupied and low-lying empty states. The available experimental reports emphasized the presence of peaks near the band edges and suggested an interpretation in terms of doublets associated with hydrogen dimers.[14,15] The KS calculations presented in ref 14 for several CNT-2H isomers identified indeed pairs of dispersionless energy bands and showed that a few high-energy configurations produced a doublet inside the energy gap of the nanotube. However, the 2(a) (ground state) was not discussed, and in the 2(b) isomer no doublet was found to lie in the gap.

An interesting scenario emerges from our calculations (performed using the PBC approach). The HOMO−LUMO

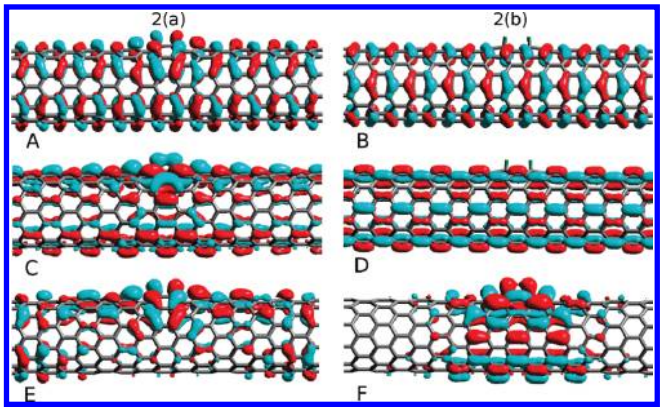

Figure 3. CNT-2H: Representative isosurfaces of the wave functions corresponding to the HOMO (A and B), LUMO (C and D), and an occupied "impurity" state (E and F) (see text). Structure 2(a) on the left; 2(b) on the right.

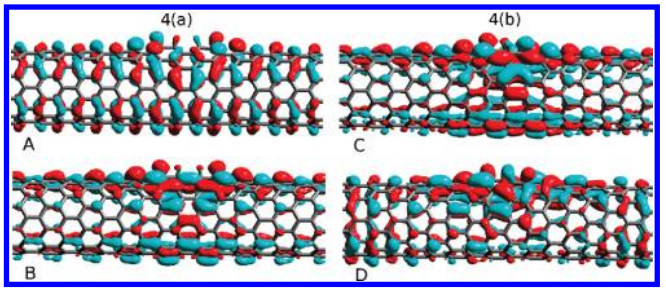

Figure 4. CNT-4H: Representative isosurfaces of the wave functions corresponding to the HOMO (A) and LUMO (B) in the 4(a) structure; and to the LUMO (C) and HOMO-2 (D) in the 4(b) structure (see text).

gap E_g of the bare CNT is 0.78 eV in the PBE calculations. A single hydrogen (CNT-1H) creates an "impurity" state in the gap, at 0.2 eV above the occupied levels of the CNT. Sparse, noninteracting hydrogens would then generate a dispersionless impurity band at that energy. On the contrary, clustering induces more complex features in the electronic energy spectrum. A doublet in the gap of the bare tube appears in 2(a), reducing E_g by 0.3 eV, but not in 2(b), where E_g remains unaltered (within 0.02 eV). Correspondingly, in 2(a) the HOMO (Figure 3A) is simply that of the bare tube bearing a perturbation at the chemisorption site, and the LUMO (Figure 3C) is a new "impurity" state mainly localized in the region where chemisorption takes place, whereas in the 2(b) geometry, both the HOMO (Figure 3B) and the LUMO (Figure 3D) bear a high resemblance with those of the bare tube, with weak amplitude at the chemisorption sites. In 2(b), an "impurity" level is identified among the unoccupied levels, at about 1.1 eV above the HOMO. Others emerge in the spectrum of the occupied levels, at 0.6 and 0.2 eV below the HOMO in 2(a) (Figure 3E) and 2(b) (Figure 3F), respectively. The 1.3 eV splitting of the impurity levels in 2(b) corresponds well with the 1.4 eV calculated in ref 14.

In the CNT-4H system, the HOMO−LUMO gap E_g is further reduced to 0.3 eV in both 4(a) and 4(b) isomers. Also, in both, the HOMO (Figure 4A for 4(a)) and the LUMO (Figure 4B for 4(a) and Figure 4C for 4(b)) are delocalized, and the LUMO has a larger amplitude in the region where chemisorption takes place. This is especially the case in 4(b). "Impurity" levels lie at about

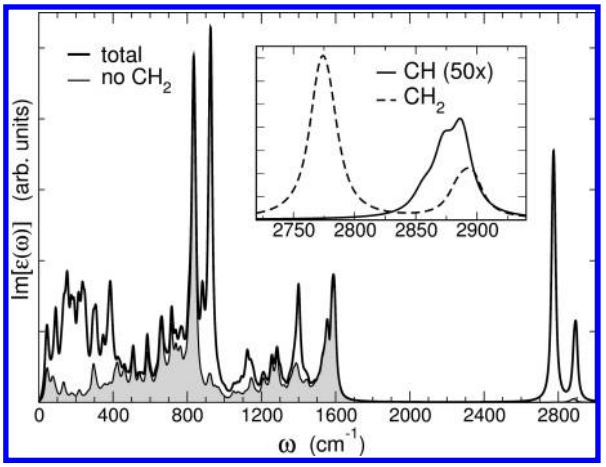

Figure 5. CNT-4H 4(a): Imaginary part of the dielectric function calculated in the harmonic approximation (see text). The inset emphasizes the structure of the highest peaks.

0.6 eV below the HOMO in both configurations (Figure 4D for 4(b)). In CNT-6H(a) and CNT-8H(a), the HOMO and LUMO, which are separated by 0.2 and 0.02 eV, respectively, share the characteristics described for the 4(a) isomer.

Despite the gap underestimate, which is intrinsic to the DFT-PBE calculations, we can conclude that the HOMO−LUMO gap tends to decrease with increasing number of the H atoms and eventually close at a critical number/concentration n_c (>8). The gap reduction is due to the progressive destabilization of the HOMOs and especially to the stabilization of the LUMOs. Note that, as one can see in Figure 4, the HOMOs have antibonding character for the π-states between the CH units, whereas the LUMOs have bonding character. Tunneling near the band edges may or may not be effective, because the levels corresponding to the states that produce higher contrast (the "impurity" levels) may or may not be at those energies, depending on the number and specific arrangement of the CH bonds.

Finally, we calculated the spectrum of the infrared-active vibrational modes of the CNT-4H (4(a)), in the harmonic approximation. We used the model with CH_2 termination, because it enables us to interpret experimental data on CNT systems[6,8] that contain not only CH units but also hydrogen atoms bonded to under-coordinated carbons at defect sites and at the ends of suspended SWNTs. The PBE results are shown in Figure 5. To investigate the effect of the "borders" overall, we have projected out their contributions; in this way, it is also possible to identify the strong contribution of the CH_2 moieties in the far-infrared (below 400 cm^{-1}).

The CH stretching modes are easily detectable as they are separated by a gap of about 1200 cm^{-1} from the top of the SWNT, which occurs at ~1600 cm^{-1} in agreement with typical IR CNT spectra.[36] The portion of the spectrum associated with CH stretching vibrations appears as bimodal; the lowest structure, with a maximum around 2780 cm^{-1}, belongs to the CH_2 groups (symmetric), whereas the highest one, with a maximum at 2890 cm^{-1}, comprises, in addition to the CH_2 groups (asymmetric), the stretching vibrations of the four CH units. Our calculations also reveal that the oscillator strengths associated with a bond in a CH_2 group involved in the two stretching modes (f_s or f_a) and that of an individual CH unit (f_1) are in the ratio $f_s:f_a:f_1$ = 12:4:1. These results are in close agreement with

dx.doi.org/10.1021/jp208501b | J. Phys. Chem. C 2012, 116, 269–275

the experimental findings of ref 8; in particular, they confirm the assignment there given and are consistent with the observed relative intensities. However, as usual, PBE predicts too soft modes. In ref 8, the vibration band extends between 2750 and 3000 cm^{-1} with peaks centered at 2850 and 2920 cm^{-1}. We note that the value of the frequency at which the highest peak is centered must depend, to some extent, on the relative numbers of CH and CH_2 groups. Other FTIR measurements[6] on SWNTs subjected to a cold plasma-generated hydrogen atoms detect this band at 2924 cm^{-1}, which is also ascribed to CH stretching modes.

Regarding the issue of "sparse" versus "clustered" configurations of the CH bonds generated by chemisorption, we can conclude that, as long as CH_2 groups are present and dominate, the overlap of their spectral features with those of the CH moieties makes it difficult to extract precise information from an IR spectrum. However, an analysis of the fine structure of the highest IR peak under controlled hydrogenation could distinguish the different contributions.

The AIREBO potential is known[37] to predict a vibrational spectrum of the tube more extended than the experimentally observed one. For the model we have considered here, CH vibrations contribute to a vast spectral range, even beyond that of the C−C stretching modes, up to 1900 cm^{-1}. Regarding the density of states corresponding to the stretching vibrations of the chemisorbed four CH's and the CH_2 groups, peaks emerge at 2870 and 2935 cm^{-1}. In contrast to our results and previous assignments,[8] the stretching modes of the CH units here are overlapping with the symmetric modes of the CH_2 groups in the lowest maximum at 2870 cm^{-1}. Therefore, while the CH moieties increase, AIREBO would suggest a change of the relative intensity of the two peaks that is inverted with respect to our predictions.

CONCLUSIONS

Our results clarify that on the exterior surface of a CNT, chemisorbed hydrogen atoms prefer ordered configurations and tend to cluster. This characteristic, which emerges from our DFT calculations, contradicts the conclusions one would draw from computations based on a classical force field (AIREBO) that favors arrangements with CH units "dispersed" and distant.[38]

Starting from the case of 2H's that strongly prefer the ortho to the para position, the pattern of energetically favored chemisorption sites on the tube is different from that predicted for graphene.[39] The AIREBO scheme, on the contrary, does not appear to capture the differences in chemical behavior related to the curvature of the nanotube as compared to graphene, which are however important for a correct description of the interaction with atomic hydrogen.[40]

DFT-PBE calculations of the dipole-allowed vibrations of a model CNT containing CH and CH_2 groups are able to characterize their contributions to the infrared spectrum measured for hydrogenated suspended SWNTs.[8] Application of the AIREBO force field to the same model reveals important discrepancies.

The analysis of our results for the electronic states at the band edges shows that their nature and their extension depend strongly on the specific structure of the adsorbate. Moreover, the HOMO−LUMO gap tends to close with increasing hydrogen concentration in the range we consider. At full coverage, however, the system is not expected to be metallic (see, e.g., ref 18), having all carbons saturated; therefore, one can also predict that a further increase of chemisorbed hydrogen will gradually drive the transformation from a "metallic" to a "semiconducting" state. This behavior deserves attention in view of the associated change one can envisage in the response of a (functionalized) nanotube when used as gas sensor.

Significant energy differences between different hydrogen configurations reflect the site-specificity in the tube. Therefore, they will then tend to diminish for increasing diameter and decreasing curvature.

The study presented was mainly focused on the search and analysis of the low-energy structures of CNT-*n*H systems. On the other hand, the measurements so far available[6,8,13,14] refer to nanotubes subjected to "aggressive" hydrogenation procedures that have probably led to kinetically driven configurations. To probe the ones thermodynamically relevant, one viable path could be hydrogenation followed by controlled thermal annealing in atomic hydrogen atmosphere.

This work is our first step within a project aimed at characterizing the chemisorption of several atomic species on the SWNTs, including the reaction dynamics.

ASSOCIATED CONTENT

Supporting Information. Atomic coordinates of all structures in Figure 1. This material is available free of charge via the Internet at http://pubs.acs.org.

AUTHOR INFORMATION

Corresponding Author
*E-mail: wanda.andreoni@epfl.ch.

ACKNOWLEDGMENT

This research was funded in part by Nano-Tera.ch, a program of the Swiss Confederation, evaluated by the SNSF. Part of the computational work was supported by a grant from the Swiss National Supercomputing Centre — CSCS under project ID 245.

REFERENCES

(1) Iijima, S. *Nature* **1991**, *354*, 56–58. Iijima, S.; Ichihashi *Nature* **1993**, *363*, 603–605. Bethune, D. S.; Klang, C. H.; De Vries, M. S.; Gorman, G.; Savoy, R.; Vazquez, J.; Beyers, R. *Nature* **1993**, *363*, 605–607.

(2) Tasis, T.; Tagmatarchis, N.; Bianco, A.; Prato, M. *Chem. Rev.* **2006**, *106*, 1105–1136. For a more recent review, see:Carbon nanotubes. *Top Appl. Phys.* **2008**, *111*, 101−164.

(3) Hirsch, A. *Angew. Chem., Int. Ed.* **2002**, *41*, 1853–1859. Campidelli, S.; Meneghetti, M.; Prato, M. *Small* **2007**, *3*, 1672–1676.Hauke, F.; Hirsch, A. In *Carbon Nanotubes and Related Structures: Synthesis, Characterization, Functionalization, and Applications*; Guldi, D. M., Martin, N., Eds.; Wiley-VCH Verlag GmbH & Co.: New York, 2010; pp 135−198.

(4) Kong, J.; Chapline, M.; Dai, H. *Adv. Mater.* **2001**, *13*, 1384–1386. Mubeen, S.; Zhang, T.; Yoo, B.; Deshusses, M. A.; Myung, N. V. *J. Phys. Chem. C* **2007**, *111*, 6321–6327. Goldoni, A.; Petaccia, L.; Lizzit, S.; Larciprete, R. *J. Phys.: Condens. Matter* **2010**, *22*, 013001–013008.

(5) Lamari Darkrim, F.; Malbrunot, P.; Tartaglia, G. P. *Int. J. Hydrogen Energy* **2002**, *27*, 193–202. Liu, C.; Chen, Y.; Wu, C.-Z.; Xu, S.-T.; Cheng, H.-M. *Carbon* **2010**, *48*, 452–455.

(6) Khare, B. N.; Meyyappan, M.; Cassell, A. M.; Nguyen, C. V.; Han, J. *Nano Lett.* **2002**, *2*, 73–77.

(7) Ruffieux, P.; Gröning, O.; Bielmann, M.; Mauron, P.; Schlapbach, L.; Gröning, P. *Phys. Rev. B* **2002**, *66*, 245416–245623.

(8) Zhang, G.; Qi, P.; Wang, X.; Lu, Y.; Mann, D.; Li, X.; Dai, H. *J. Am. Chem. Soc.* **2006**, *128*, 6026–6027.

(9) Nikitin, A.; Li, X.; Zhang, Z.; Ogasawara, H.; Dai, H.; Nilsson, A. *Nano Lett.* **2008**, *8*, 162–167.
(10) Yoshihara, K.; Ishida, K.; Wongwiriyapan, W.; Inoue, S.; Okabayashi, Y.; Honda, S.; Nishimoto, Y.; Kuwahara, Y.; Oura, K.; Katayama, M. *Appl. Phys. Express* **2008**, *1*, 094001–094003.
(11) Chen, Z.; Thiel, W.; Hirsch, A. *ChemPhysChem* **2004**, *4*, 93–97.
(12) Barone, V.; Heyd, J.; Scuseria, G. E. *J. Chem. Phys.* **2004**, *120*, 7169–7173.
(13) Han, S. S.; Lee, H.-M. *Carbon* **2004**, *42*, 2169–2177.
(14) Buchs, G.; Krasheninnikov, A. V.; Ruffieux, P.; Gröning, P.; Foster, A. S.; Nieminen, R. M.; Gröning, O. *New J. Phys.* **2007**, *9*, 275–286.
(15) Nikitin, A.; Zhang, Z.; Nilsson, A. *Nano Lett.* **2009**, *9*, 1301–1306.
(16) Yildirim, T.; Gülseren, O.; Ciraci, S. *Phys. Rev. B* **2001**, *64*, 075404–075408.
(17) Lee, S. M.; Lee, Y. H. *Appl. Phys. Lett.* **2000**, *76*, 2877–2879.
(18) Lee, S. M.; An, K. H.; Lee, Y. H.; Seifert, G.; Frauenheim, T. *J. Am. Chem. Soc.* **2001**, *123*, 5059–5063.
(19) Gülseren, O.; Yildirim, T.; Ciraci, S. *Phys. Rev. B* **2002**, *66*, 121401–121404.
(20) Fan, W. J.; Zhang, R. Q.; Teo, B. K.; Aradi, B.; Frauenheim, T. *Appl. Phys. Lett.* **2009**, *95*, 013116–013118.
(21) Heyd, J.; Scuseria, G. E.; Ernzerhof, M. *J. Chem. Phys.* **2003**, *118*, 8207–8215.
(22) Perdew, J. P.; Burke, K.; Ernzerhof, M. *Phys. Rev. Lett.* **1996**, *77*, 3865–3868. **1998**, *80*, 891–894.
(23) Becke, A. D. *Phys. Rev. A* **1988**, *38*, 3098–3100. Lee, C.; Yang, W.; Parr, R. G. *Phys. Rev. B* **1988**, *37*, 785–789.
(24) Adamo, C.; Barone, V. *J. Chem. Phys.* **1999**, *110*, 6158–69.
(25) Brenner, D. W.; Shenderova, O. A.; Harrison, J. A.; Stuart, S. J.; Ni, B.; Sinnott, S. B. *J. Phys.: Condens. Matter* **2002**, *14*, 783–802.
(26) This model was previously used in: Vitale, V.; Curioni, A.; Andreoni, W. *J. Am. Chem. Soc.* **2008**, *130*, 5848–5849.
(27) Troullier, N.; Martins, J. L. *Phys. Rev. B* **1991**, *43*, 1993–2006.
(28) Billeter, S. R.; Curioni, A.; Andreoni, W. *Comput. Mater. Sci.* **2003**, *27*, 437–445.
(29) Giannozzi, P.; De Gironcoli, S.; Pavone, P.; Baroni, S. *Phys. Rev. B* **1991**, *43*, 7231–7242.
(30) *CPMD V3.13.3*; Copyright IBM Corp. 1990−2011; MPI für Festkörperforschung: Stuttgart, Germany, 1997−2001.
(31) Hockney, R. W. *Methods Comput. Phys.* **1970**, *9*, 136–211.
(32) Zhao, Y.; Truhlar, D. G. *Acc. Chem. Res.* **2008**, *41*, 157–167.
(33) Valiev, M.; Bylaska, E. J.; Govind, N.; Kowalski, K.; Straatsma, T. P.; van Dam, H. J. J.; Wang, D.; Nieplocha, J.; Apra, E.; Windus, T. L.; de Jong, W. A. *Comput. Phys. Commun.* **2010**, *181*, 1477–1489.
(34) Plimpton, S. J. *J. Comput. Phys.* **1995**, *117*, 1−19, http://lammps.sandia.gov.
(35) We use the definition in: Haddon, R. C. *J. Am. Chem. Soc.* **1997**, *119*, 1797–1798.
(36) Kastner, J.; Pichler, T.; Kuzmany, H.; Curran, S.; Blau, W.; Weldon, D. N.; Delamesiere, M.; Draper, S.; Zandbergen, H. *Chem. Phys. Lett.* **1994**, *221*, 53–58.
(37) Lindsay, L.; Broido, D. A. *Phys. Rev. B* **2010**, *81*, 205541–205546.
(38) See e.gMuniz, A. R.; Singh, T.; Maroudas, D. *Appl. Phys. Lett.* **2009**, *94*, 103108–103110. Muniz, A. R.; Maroudas, D. *J. Appl. Phys.* **2010**, *108*, 113532–113541. Despite the claimed agreement with non-specified DFT calculations of hydrogen pairs on a CNT, the reported graphical representations of the results of the AIREBO simulations are fully consistent with our findings.
(39) Boukhvalov, D. W.; Katsnelson, M. I. *Phys. Rev. B* **2008**, *78*, 085413–085417.
(40) This conclusion does not affect the validity of studies of H_2 physisorption by CNTs carried out using the AIREBO potential, for example: Knippenberg, M. T.; Stuart, S. J.; Cheng, H. *J. Mol. Model.* **2008**, *14*, 343–351.